Progress In Electromagnetics Research B, Vol. 42, 75–91, 2012

MULTIMODE BEHAVIOR OF A 42 GHz, 200 kW GYROTRON

Ashutosh*, B. Ravi Chandra, and P. K. Jain

Centre of Research in Microwave Tubes, Department of Electronics Engineering, Institute of Technology, Banaras Hindu University, Varanasi-221005, India

Abstract—The multimode beam-wave interaction behavior in a tapered, cylindrical cavity RF interaction structure of a 42 GHz gyrotron operating in the TE_{03} mode has been investigated through nonlinear analysis and PIC simulation. A technique for producing the annular gyrating electron beam in PIC simulation code CST Particle Studio has been described. An energy transfer phenomenon from electron beam to RF has been demonstrated. The performance of cavity has been monitored to ensure the device operation in the desired mode and frequency. In the PIC simulation, the effect of beam velocity spread on the power output has been illustrated. Using multimode behaviour, the effect of presence of nearby modes on the cavity performance has been observed. The simulation results have been compared with the results obtained from self-consistent single-mode analysis and time-dependent multimode analysis. It has been found that output power is well above the desired 200 kW level for the designed 42 GHz gyrotron operating in TE_{03} mode.

1. INTRODUCTION

Among the existing gyro-devices, gyrotron oscillator is a reliable and considerably efficient source to produce high power both in pulse and CW operation ranging from microwave to sub-millimeter wavelength [1–3]. Gyrotron has application in a variety of systems including radars, materials processing and medical imaging, etc. [4, 5]. However, gyrotrons are more attractive for the applications in electron cyclotron resonance plasma heating (ECRH) in tokamak and

Received 9 May 2012, Accepted 26 June 2012, Scheduled 27 June 2012

* Corresponding author: Ashutosh (asingh.rs.ece@itbhu.ac.in).

stellerator systems, electron cyclotron current drive (ECCD), stability control and diagnostics of magnetically confined plasmas for generation of energy by controlled thermonuclear fusion, and DNP/NMR/ESR spectroscopy [4, 5].

Gyrotron is a CRM based vacuum electron beam device that involves fast wave interaction between RF electromagnetic and space charge cyclotron waves on the annular gyrating electron beam in a smooth wall RF interaction structure [1–3]. To achieve high power at higher frequency, the gyrotron has to operate necessarily at higher order mode to alleviate the problem of wall heating and beam interception due to miniaturization of interaction structure at these frequencies. At the higher order mode of operation, the mode spectrum is dense and electron beam is likely to interact with several modes in the cavity that lead to unstable device operation and lower efficiencies [2, 3, 6, 7]. Additionally, to reduce the high DC magnetic field requirement, gyrotrons are often operated in higher harmonics which also leads to mode competition from nearby competing modes and the lower harmonic modes [8, 9]. Hence, for a high efficiency gyrotron, it is a challenging task to avoid the mode competition. Mode interaction theory has been presented in many of the literatures in the past [1, 3, 6, 7]. In fact, the single mode operation is possible if the design of interaction structure is appropriate and the start oscillation current criteria are suitably analyzed for the designed cavity. For these devices multimode theory is used to predict accurate power and efficiency which incorporates the effect of presence of all nearby modes inside the cavity. Both, linear and nonlinear analyses of the gyrotrons have been well described in the literatures [1–3, 10–14]. On the other hand, PIC simulation offers insight into the beam-wave interaction phenomena in the gyrotrons [15–17].

A 42 GHz, 200 kW CW gyrotron is currently under development for electron cyclotron resonance plasma heating application in India. The objective of this paper is to investigate the RF behavior of tapered cylindrical interaction structure of this 42 GHz gyrotron in the presence of all competing modes. Nonlinear single-mode analysis of the 42 GHz gyrotron and its PIC simulation using commercial code, MAGIC, was performed earlier to study its beam wave interaction mechanism [12, 15]. In the present work, nonlinear time-dependent multimode analysis of a 42 GHz gyrotron and its PIC simulation using CST particle studio code are done to observe the multimode beam-wave interaction behavior. The gyrating beam emission command is not available in the CST PIC particle studio code; a special arrangement is used here to emulate a gyrating electron beam emission from the MIG-type cathode required for the beam-wave interaction. The field

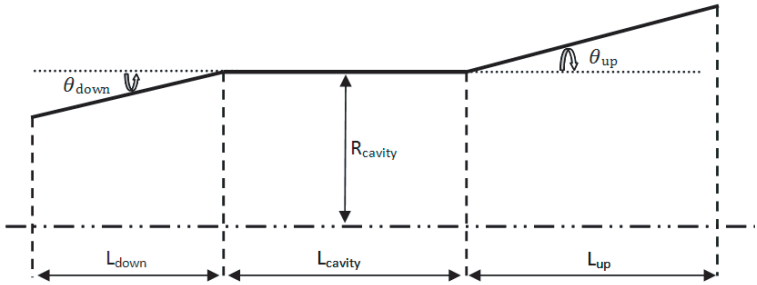

Figure 1. Schematic of a tapered cylindrical interaction structure of a gyrotron.

values are recorded in the time domain and its Fourier transform is obtained which provides the device operating frequency. The electron particle beamlets at different time intervals within one cycle are shown to understand the bunching mechanism. The energy distribution of all the particles along the interaction length is also observed to describe the energy transfer phenomena. Beam-wave interaction yields the temporal RF power growth at the output end of the interaction structure. The stability of device performance is also discussed. To study the performance of the overmoded cavities in the presence of several modes, a multimode theory is presented based on the formulation developed by Fliflet et al. [14]. The comparisons of results obtained through the single-mode and multimode analyses as well as from the simulations are also discussed.

2. GYROTRON RF INTERACTION STRUCTURE

The gyrotron RF interaction cavity used is a three-section structure consisting of a central smooth wall cylindrical waveguide section along with two linear-tapered cylindrical waveguide sections, down taper at the entrance and up taper at the output (Figure 1). Both up and down taper sections of the cavity provide enough reflection to maintain a standing wave pattern in the main central section of the cavity. Input down taper section ensures the cut-off condition which prevents the back propagation of RF power towards the gun region. The beam-wave interaction takes place in the uniform middle section where the RF field attains its maximum value. Up taper section of the cavity converts the standing wave into travelling wave to transfer cavity energy to the output [1]. The typically selected geometry parameters for the present work are listed in Table 1 [12].

Table 1. Structure parameter of tapered cavity.

Parameters	Value
L_{down}	30 mm
L_{cavity}	44 mm
L_{up}	46 mm
θ_{down}	2°
θ_{cavity}	0°
θ_{up}	3°

Table 2. Design specifications of 42 GHz, 200 kW gyrotron [12].

Particulars	Specifications
Mode	TE_{03}
Beam voltage (V_b)	65 kV
Beam current (I_b)	10 A
Velocity ratio	1.4
Magnetic field (B_0)	1.61-1.62 T
Wall radius (R_0)	11.57 mm
Beam radius (R_b)	6.06 mm
Harmonic number (s)	1 i.e., fundamental mode
Output power	200 kW
Efficiency	30.7%
Wall loading	$< 2.0\,\mathrm{kW/cm^2}$
L/λ	6.3
Diffractive Q	840

3. START OSCILLATION CURRENT

Start oscillation current is the minimum current required to start the oscillations in gyrotron. To observe the nearby competing modes of the design mode, start oscillation current calculation is required. For typically selected design parameters of the present 42 GHz gyrotron as given in Table 2, the starting currents are computed using the linearized single-mode theory [10]. From Figure 2, it could be observed that for the required operating TE_{03} mode there are two important competitors, TE_{23} and TE_{52}, which might couple to electron beam and start oscillating.

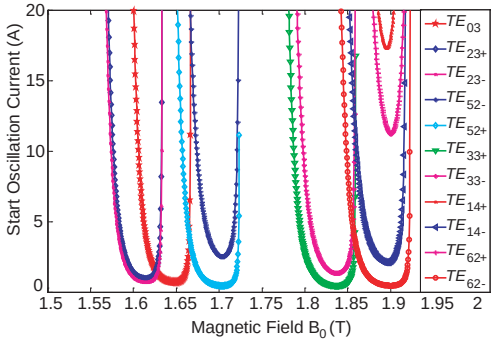

Figure 2. Start oscillation current as a function of magnetic field for various modes with the beam radius optimized for TE_{03} mode.

4. TIME-DEPENDENT MULTIMODE ANALYSIS

A time-dependent, nonlinear, multimode theory is adopted here as formulated by Fliflet et al. [14] to estimate the output power for the 42 GHz gyrotron oscillator. Multimode analysis provides the evolution of complete beam-wave interaction of the device and accounts the effect of different competing modes with irregularly spaced frequencies and unequal coupling impedances on the device performance. In this approach, mode amplitudes (a_n) and phases Ψ_n are solved from coupled, nonlinear, time-dependent equations of the form [14];

$$\frac{da_n}{dt} + \frac{\omega_o a_n}{2Q_n} = -\frac{1}{2\varepsilon_0} * \mathrm{Im} P_n(t) \tag{1}$$

$$\frac{d\psi_n}{dt} + \omega_0 = \omega_{n0} - \frac{1}{2\varepsilon_0 a_n} * \mathrm{Re} P_n(t) \tag{2}$$

where, ω_{n0} is the cold-cavity eigenfrequency of the mode, ω_0 a reference frequency, Q_n the mode quality factor, and ε_0 the free-space permittivity. P_n, the complex, slow-time-scale component of the electron beam polarization for the mode n, is given as;

$$P_n(t) = \frac{i}{W} \int_V dS\, dz\, h(z)\, e_n^* \cdot j_\omega\, e^{i\psi_n} \tag{3}$$

i denotes the imaginary unit, W an expression defined as $W = \int_0^L dz \left|h(z)^2\right|$, and $j_\omega = \int_0^{2\pi} d(\omega_0 t) j_t e^{i\omega_0 t}$ the Fourier transform of the transverse current density j_t. Here, dS is infinitesimal area element of waveguide's cross section perpendicular to its axis, $h(z)$ is the axial

field profile, $e_n(= \hat{z} \times \nabla_t \varphi_n)$ is the transverse vector function for a TE mode. φ_n is the scalar function and is defined as (for a circular waveguide)

$$\varphi_n = C_{m_n l_n} J_{m_n}(k_{m_n l_n} r) \exp i(m_n \theta) \tag{4}$$

where, J_{m_n} is Bessel function of first kind of argument $k_{m_n l_n} r$. $k_{m_n l_n} = X_{m_n l_n}/r_w$ where, $X_{m_n l_n}$ is the eigenvalue and r_w is the cavity wall radius. The coupled Equations (1) and (2) have been integrated using the Runge-Kutta method. Each mode has to be assigned small initial amplitude with arbitrary phase to start the numerical integration. The coupled equations are integrated for each mode iteratively at each time step. The knowledge of amplitude and phase leads to the evaluation of output power growth in time domain. Mode amplitudes converge to self-consistent values as soon as the electrons transfer their energy to RF and this happens within few time steps in the simulation. The convergence of mode amplitude also depends upon the ramp up of the beam-energy and pitch factor.

5. PIC SIMULATION DESCRIPTION

CST particle studio is a module for carrying out simulation of interaction between electromagnetic fields and charged particles. It is based on the finite integration method and uses hexahedral/tetrahedral meshing for discretizing the computational domain [18]. It gives an insight into the EM behavior of the high frequency designs with more user friendly interface. Diagnosis of results and its post-processing module are its salient features. Another PIC code MAGIC is a user configurable code based on finite-difference time-domain method (FDTD) method [19] while CST particle studio is GUI based 3D simulation code [18]. In the MAGIC, output power corresponding to only one mode can be observed and it is not possible to observe the power levels of the other modes present in the output temporal signal. On the other hand, CST particle studio has provision to observe the signal growth and output powers corresponding to all the modes present in the output. The basic steps in simulating RF interaction structure in the presence of electron particles using PIC solver of "CST Particle Studio" are described in the following section.

5.1. RF Interaction Cavity Modeling

A 3D model of an all-metal, tapered cylindrical cavity used for PIC simulation in the beam present case is shown in Figure 3(a). Material property of the cavity wall is typically considered as copper with conductivity 5.7×10^7 S/m and its background material is

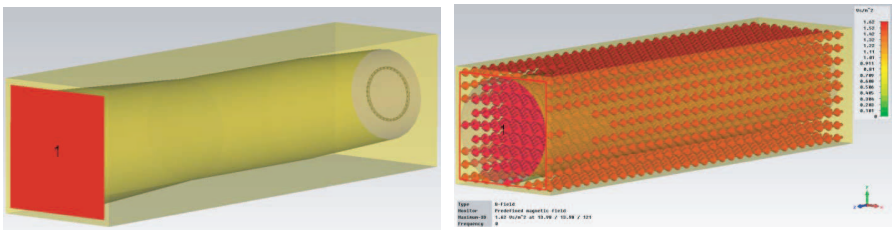

(a) (b)

Figure 3. (a) 3-D view of an all-metal, cylindrical tapered cavity used in simulation and (b) magnetic field intensity distribution along the interaction structure (Copper is used as structure material and background material is normal).

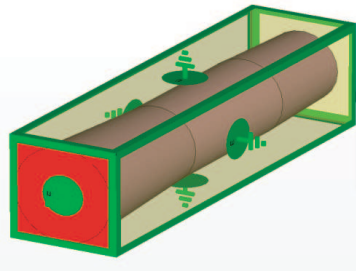

Figure 4. Boundary conditions implementation around the tapered cavity.

kept normal (vacuum). In practice, the conductivity of cavity wall material is kept high to reduce the ohmic loss. Moreover, the conductivity does not affect significantly the total quality factor. In the simulation, conductivity value has to be defined, hence such a value has been typically selected. The diffractive Q does not depend on the conductivity value since it is reserved for the axial loss due to the open cavity and provides a method of power extraction. A port is assigned at the output taper end to observe the signal of any mode (Figure 3(a)). Some of the results can be obtained using post processing feature of the software. The constant DC magnetic field is applied along the interaction structure as shown in Figure 3(b).

In the simulation, finite dimension structure needs to be assigned suitable boundary condition as per problem concerned. The boundary conditions are made electric ($E_t = 0$) along all six faces of the bounding box as shown in Figure 4. Proper meshing should be made for the structure discretization to obtain good results. Here, hexahedral

meshing is used which is very robust even for most complex imported geometries and allows very fast computations with good accuracy. In Figure 5, red dot represents mesh node at a particular position and mesh lines pass through these nodes. Lines per wavelength control the size of mesh shells. Mesh line ratio limit determines the limitation for the smallest mesh step choice [18].

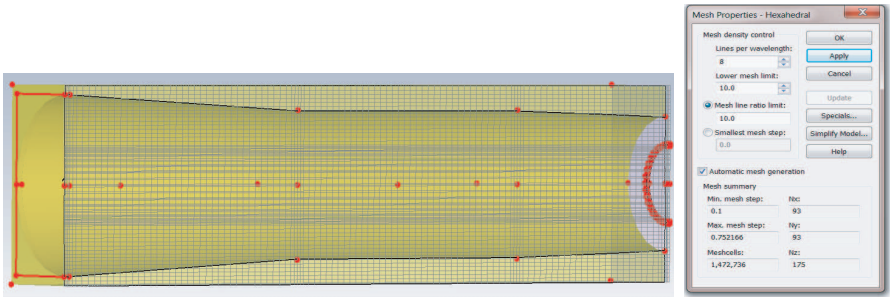

Figure 5. Mesh view of simulation structure with mesh properties.

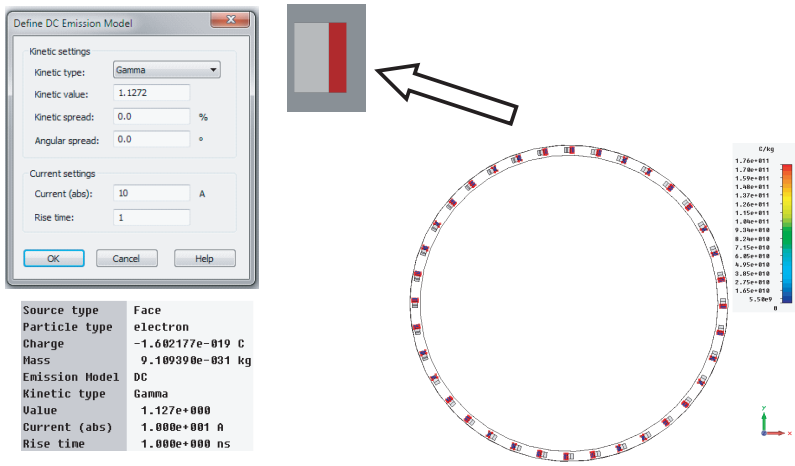

Figure 6. Design of cathode with emitters (indicated by arrow) to produce the gyrating electron beamlets injected into the interaction structure to drive the oscillations. The DC emission model dialogue box is also shown (beam parameters specified in Table 2).

5.2. Particle Emission Model

For the beam-wave interaction, the gyrating electron beam is introduced into the tapered cavity to drive the electromagnetic oscillations from the noise background. There are no tools for generating gyrating electron beam. A special arrangement is used to produce the gyrating electron beam as shown in Figure 6. Particles are emitted from a tilted surface whose angle of tilt is determined from the ratio of transverse velocity of the beam to the axial velocity. The cathode has the radius same as that of the beam radius. Initially, all the particles have been assigned a constant energy value and the current rise time is taken as 2 ns. A kinetic spread for the beam and current is defined based on the quality of the beam obtained separately by analysis/simulation of a magnetron injection gun (MIG). For the accuracy of results, more than 12 numbers of particle beamlets should be considered. Monitors for fields are set to observe the cavity operation in desired mode and frequency. The particles are monitored at a set interval of time over the entire or part of simulation time for their momentum, position etc. This stores the full particle data at the set location, which can be exported for subsequent simulation of collector. For the analysis of electron bunch and energy transfer phenomena, phase space for momentum and position of electrons is recorded.

6. RESULTS AND DISCUSSION

In the beam present case, a gyrating electron beam of 65 keV energy and transverse-to-axial velocity ratio (α) = 1.4 is introduced at the input end of the tapered cylindrical RF interaction cavity. With a beam radius of 6.06 mm, electron beam gets coupled to the second radial maximum of the operating TE_{031} mode in the resonator.

6.1. Electron Beam Bunching

The electrons interact self-consistently with RF field in the straight section. The RF field action changes the electron relativistic factor (γ), depending on the electron phase relative to the wave, and results in phase slippage and bunching, with the corresponding current driving the wave in turn. The snapshot of all the particles before and after the RF interaction inside the resonator is shown in Figures 7(a) and 7(b). Before interaction, all 36 beamlets are uniformly distributed with the fixed guiding center radius and their energies are equal at the starting of interaction process. The Figure 7(a) also shows that the Larmor radius of all beamlets is same. In Figure 7(b), bunching of particles

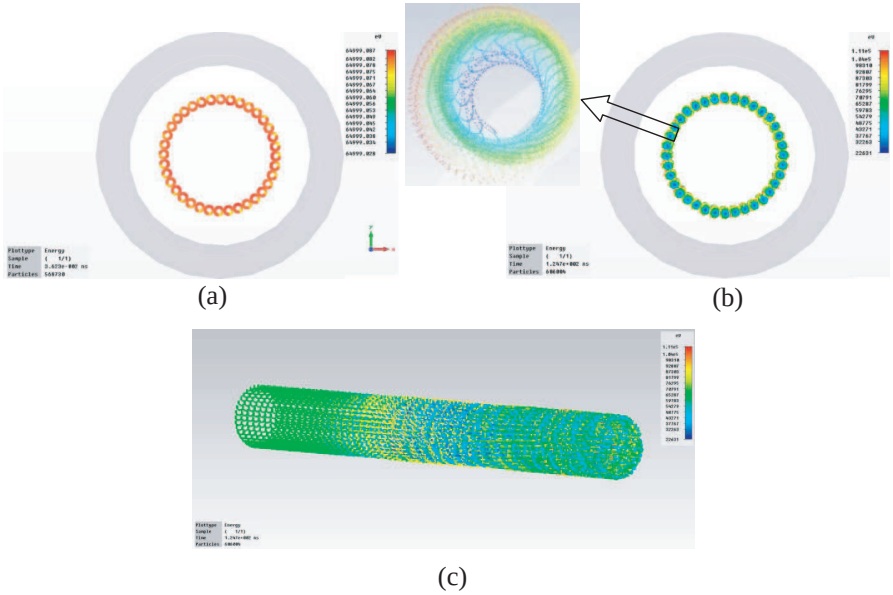

Figure 7. Front view of electron beam with 36 beamlets (a) before interaction, (b) after interaction (inset shows a zoomed beamlet), and (c) side view of all the particles along the cavity after the interaction.

is clearly shown in the zoomed beamlet which is observed due to the change in the Larmour radius during the beam-wave interaction process. Figure 7(c) shows the trajectory of all the particles along the interaction length. Obviously, the presence of RF field perturbs the homogeneity of helical electron beamlets in the straight section and results in an electron bunch formation. This bunch slips in to the retarding phase of field, and hence transfers energy to the RF field.

6.2. RF Field Pattern

After the interaction, electric field at 42 GHz is monitored and TE_{03} mode of operation is observed. In Figure 8(a), the electric field at a transverse cross section in the straight section is shown. In Figure 8(b), electric field at a cross section along the cavity length is shown. It can be explicitly seen that RF strongly resonates in the straight section forming a standing wave. At the input taper side, no propagation of RF is observed while in the output taper region, RF field is present and is partially travelling. The quantitative variation of electric field is shown in Figures 8(c) and 8(d) along radial and axial direction.

Figure 8(c) confirms TE_{03} mode of operation with 3 variations along the radius and electron beam radius coincides with the second radial maximum. In Figure 8(d), maximum electric field is observed in the cylindrical straight section. It is almost zero at the input taper side while a lower and finite value in the uptaper side value is obtained due to partial propagation of the field. This diffracted RF is coupled to window of the gyrotron.

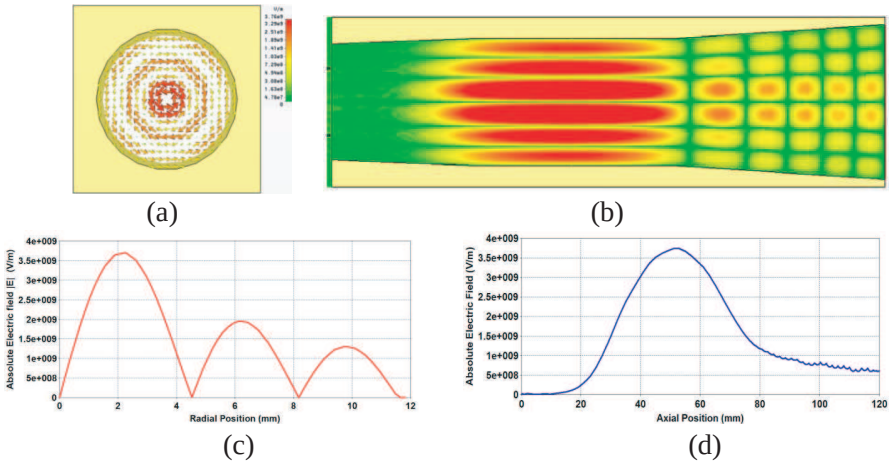

Figure 8. (a) Vector plot of electric field profile at middle of straight-section, (b) contour plot of electric field along the cavity length. Variation of absolute electric field along (c) radial and (d) axial direction.

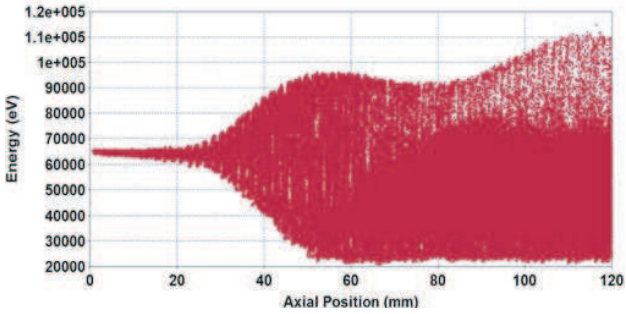

Figure 9. Energy distribution of all the electrons along the axis of interaction structure.

6.3. RF Signal Generation and Power Output

Energy distribution of all electrons is shown in Figure 9. Initially, all electrons have same energy of 65 keV. But with the time, energy of particles gets perturbed due to the interaction with RF present in the cavity. Majority of particles have lower energy at the end of interaction region. This represents that particles have lost their energy to RF field as they come out of resonator and a net energy transfer from electrons to the RF field.

The simulation results of beam wave interaction are shown in Figure 10. The temporal profile of field amplitude of all the nearby modes including TE_{03} mode at the output end of the cavity is shown in Figures 10(a) and 10(b) for different DC magnetic fields values. Obviously, the output time signal corresponding to TE_{03} mode has the highest amplitude than all other modes in both cases. Mode competition is observed mainly due to TE_{23} mode at lower magnetic fields for the present design (Figure 2). It can be seen from the Figure 10(a) that initially, the signal corresponding to TE_{23} mode starts growing readily compared to TE_{03} mode, but finally after 120 ns, TE_{23} signal decays and TE_{03} signal starts growing. There is a stiff

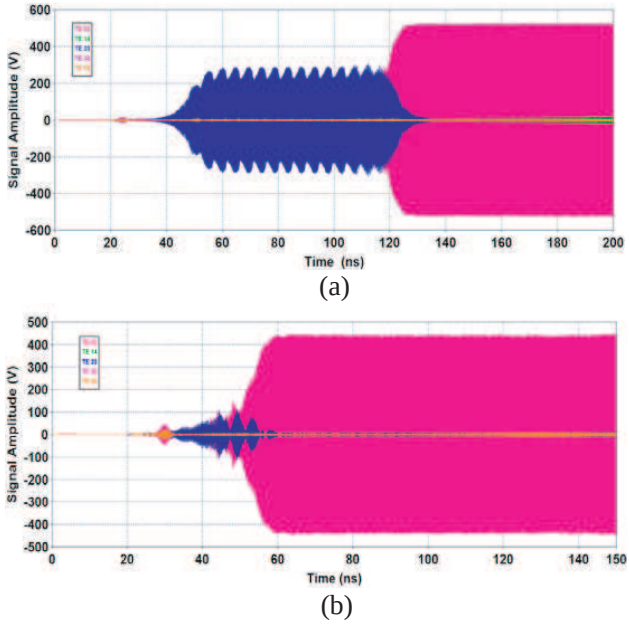

Figure 10. Temporal response of output signals for TE_{03} and its nearby competing modes for magnetic field (a) $B_0 = 1.61$ T and (b) $B_0 = 1.62$ T.

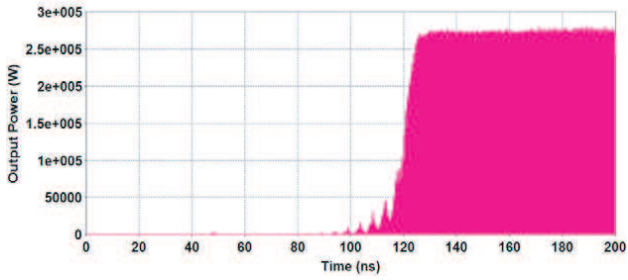

(a)

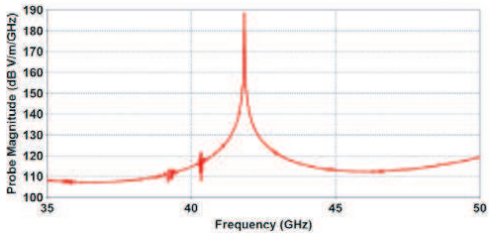

(b)

Figure 11. (a) Temporal output power growth at output end of the cavity for TE_{03} mode and (b) frequency spectrum of probe signal.

competition between these two modes for 1.61 T magnetic field but ultimately TE_{03} mode gets established in the cavity. In Figure 10(b), for 1.62 T magnetic field, the increase in the amplitude of TE_{23} mode is lower than previous case and it decays faster after 60 ns. On the other hand, TE_{03} mode stabilizes around 60 ns in the cavity and becomes stable. The maximum steady state signal amplitude observed corresponds to TE_{03} mode at $B_0 = 1.61$ T. Below 1.61 T magnetic field, cavity oscillates in TE_{23} mode. RF power saturates around 120 ns with 270 kW and 46% efficiency (Figure 11(a)). A probe is placed inside the cavity at the position of maximum electric field and its signal is recorded in time domain. The Fourier transform of this signal shows a single frequency of oscillation at 42 GHz (Figure 11(b)).

6.4. Parametric Analysis and Validation

Using the PIC simulation, the output power variation has been observed with the static magnetic field and with beam velocity ratio for different velocity spreads. Obviously, with increasing velocity spread, the output power decreases (Figure 12). This happens because some particles have lower velocities and hence transfer lesser amount of energy to the RF.

In Figure 13, temporal growth of output power is shown for the

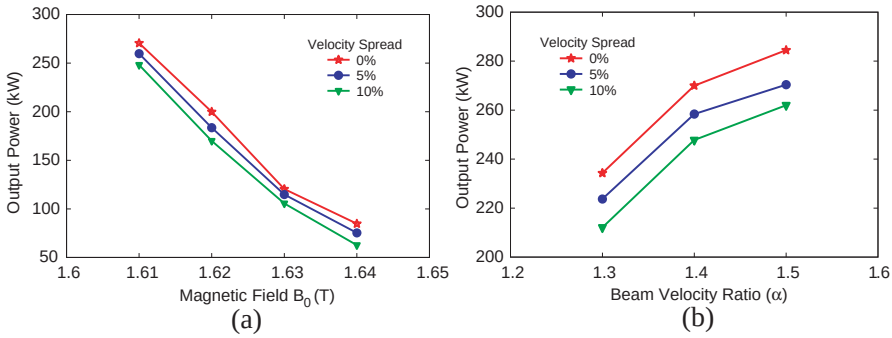

Figure 12. Output power variation with (a) magnetic field and (b) beam velocity ratio (α) for different velocity spreads.

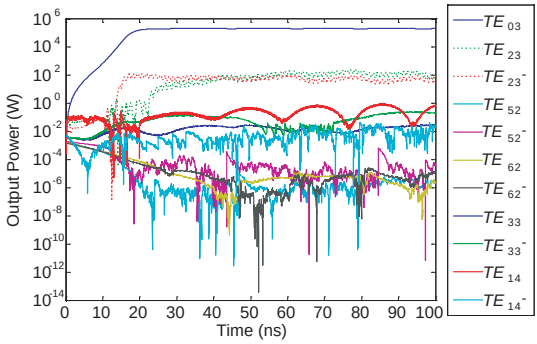

Figure 13. Temporal growth of output power for designed TE_{03} mode and all the probable competing modes at magnetic field $B_0 = 1.615\,\mathrm{T}$.

desired TE_{03} mode and possible nearby modes obtained from the multimode analysis. Obviously, maximum power growth is observed in TE_{03} mode and other modes contain much less output RF power, similar to that observed through PIC simulation (shown in Figure 10). The difference in the saturation time of TE_{03} mode in the analysis ($\sim$ 20 ns) and simulation ($\sim$ 60 ns) is probably because of the consideration that the time scale on which amplitude and phase of a mode change in the cavity is much larger than the time scale on which a particle's orbit is changed, which reduces the computation time considerably. Whereas, in CST Particle Studio, there is no provision to exploit the order of time scales and it simulates the interaction process more naturally, accurately and self-consistently. The output power is obtained well above the desired 200 kW for the magnetic field 1.615 T. The applied DC magnetic field is kept constant with time. The output power is also calculated with varying DC magnetic field. The output powers calculated using single-mode and multimode

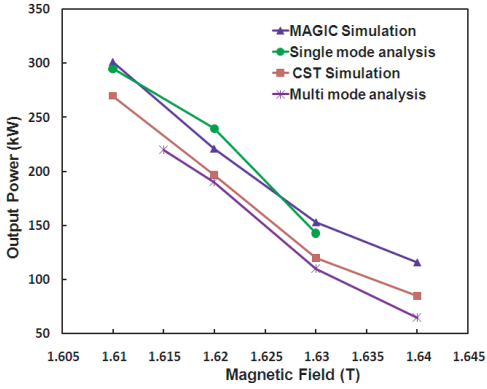

Figure 14. Comparison of output power results obtained from PIC simulations, single and multimode analyses for different DC magnetic fields.

analysis are compared with the simulation results obtained from CST and MAGIC code (Figure 14). It can be seen that results obtained from single-mode analysis and MAGIC are in close agreement but they differ (higher) from that obtained from CST particle studio PIC simulation and multimode analysis by $\sim 15\%$. CST particle studio PIC simulation code accounts for the multimode oscillations present in the RF cavity and the RF power growth in all the other nearby modes can be observed similar to multimode analysis. Moreover, the RF power growth obtained from CST particle studio simulation code and multimode analysis is in close agreement with only $\sim \pm 4\%$ variation. As the presence of competing modes is inevitable in a conventional cavity, consideration of the nearby competing modes provides more realistic picture of the beam-wave interaction mechanism. Obviously, for the present design of gyrotron, output power is obtained well above the desired 200 kW power level at around 38% efficiency.

7. CONCLUSION

An investigation of RF behavior of a conventional, tapered, cylindrical cavity RF interaction structure for a 42 GHz CW gyrotron has been presented using the multimode analysis and PIC simulation. Start oscillation current diagram provides the possible mode competitors to the TE_{03} mode. Steps involved in the PIC simulation have been described. Electric field patterns that have been obtained through simulation confirm the operation in the designed mode. The maximum of field has been observed in the straight cylindrical section which is essential for the maximum energy transfer during the beam-wave

interaction. Field coupling to output through the uptaper section has also been observed. A novel scheme is used to produce the gyrating electron beam for the beam-wave interaction. Beamlets observed at the end of simulation shows the bunching phenomena of the particles. The energy distribution of all the particles along the interaction length shows a net energy transfer from electron beam to RF. The cavity takes some time to settle in the TE_{031} mode due to the competition from nearby modes. After 120 ns, a stable 270 kW output power has been obtained. The frequency spectrum of the recorded field has a single peak at 42 GHz that shows the device is strongly intended to operate at 42 GHz resonant frequency. Consideration of the velocity spread of the electron beam lowers the power output. The multimode effect on the performance of the device has been presented and a decrease in output power has been observed in comparison to single-mode results. Output power has been compared with the analytical results obtained by self-consistent single-mode nonlinear analysis and multimode analysis and in all the results the output power is well above the desired 200 kW level.

ACKNOWLEDGMENT

One of the authors (Ashutosh) is thankful to Centre of Advanced Studies (University Grant Commission), Department of Electronics Engineering, IT-BHU, for financial support.

REFERENCES

1. Edgcombe, C. J. (ed.), *Gyrotron Oscillators: Their Principles and Practice,* Taylor and Francis Ltd., London, 1993.
2. Kartikeyan, M. V., E. Borie, and M. K. Thumm, *Gyrotrons High-Power Microwave and Millimeter Wave Technology*, Springer, Germany, 2004.
3. Nusinovich, G. S., *Introduction to the Physics of Gyrotrons*, Johns Hopkins University Press, Baltimore, 2004.
4. Thumm, M. K., "State-of-the-art of high power gyro-devices and free electron masers update 2009," Scientific Reports FZKA 7467, Forschungszentrum Karlsruhe, Karlsruhe, Germany, 2010.
5. Eichmeier, J. A. and M. K. Thumm, *Vacuum Electronics — Components and Devices*, Springer, New York, 2008.
6. Kreischer, K. E., R. J. Temkin, H. R. Fetterman, and W. J. Mulligan, "Multimode oscillation and mode competition in

high-frequency gyrotrons," *IEEE Trans. Microwave Theory Tech.*, Vol. 32, 481–490, 1984.

7. Nusinovich, G. S., "Review of the theory of mode interaction in gyrodevices," *IEEE Trans. Plasma Science*, Vol. 27, No. 2, 313–326, Jun. 1999.
8. Chu, K. R., "Theory of electron cyclotron maser interaction in a cavity at the harmonic frequencies," *Phys. Fluids*, Vol. 21, 2354–2364, 1978.
9. Liu, P. K. and E. Borie, "Mode competition and self-consistent simulation of a second harmonic gyrotron oscillator," *Int. J. Infrared Millimeter Waves*, Vol. 21, No. 6, 855–882, 2000.
10. Kreischer, K. E. and R. J. Temkin, "Linear theory of an electron cyclotron maser operating at the fundamental," *Int. J. Infrared Millimeter Waves*, Vol. 1, No. 2, 195–223, Jun. 1980.
11. Danly, B. G. and R. J. Temkin, "Generalized nonlinear harmonic gyrotron theory," *Phys. Fluids*, Vol. 29, 561–567, 1986.
12. Kartikeyan, M. V., A. Kumar, S. Kamakshi, P. K. Jain, S. Illy, E. Borie, B. Piosczyk, and M. K. Thumm, "RF behavior of a 200-kW CW gyrotron," *IEEE Trans. Plasma Science*, Vol. 36, No. 3, 631–636, Jun. 2008.
13. Fliflet, A. W., M. E. Read, and K. R. Chu, "A self-consistent field theory for gyrotron oscillators: Application to a low Q gyromonotron," *Int. J. Electron.*, Vol. 53, No. 6, 505–521, Dec. 1982.
14. Fliflet, A. W., R. C. Lee, S. H. Gold, W. M. Manheimer, and E. Ott, "Time-dependent multimode simulation of gyrotron oscillators," *Phys. Rev. A*, Vol. 43, No. 11, 6166–6176, Jun. 1991.
15. Reddy, D. M., A. K. Sinha, and P. K. Jain, "Eigenmode and beam-wave interaction simulation for small orbit gyrotron using MAGIC," *International Conference on Microwaves, Antenna, Propagation & Remote Sensing, ICMARS,* Jodhpur, Feb. 2008.
16. Wu, H., R. L. Liou, and A. H. McCurdy, "PIC code simulation of pulsed radiation in a tapered closed-cavity gyrotron," *IEEE Trans. Plasma Science*, Vol. 24, No. 3, 606–612, Jun. 1996.
17. Reddy, S. U. M., V. B. Naidu, S. K. Datta, P. K. Jain, and L. Kumar, "PIC simulation of a gyrotron-traveling-wave tube amplifier," *IEEE International Vacuum Electronics Conference (IVEC)*, 319–320, 2010.
18. CST-Particle Studio, *User's Manual,* Darmstadt, Germany, 2011.
19. *MAGIC User's Manual: 2007 Version of Magic 3D*, ATK Mission Research, Washington, 2007.